

Probing the metastability of a protoneutron star with hyperons in a core-collapse supernova

Sarmistha Banik*

BITS Pilani, Hyderabad Campus, Hyderabad 500078, India

(Received 13 December 2013; revised manuscript received 28 January 2014; published 25 March 2014)

The role of Λ hyperons is investigated in the dynamical collapse of a nonrotating massive star to a black hole using a one-dimensional general-relativistic (GRID) code. The dynamical formation and evolution of a protoneutron star (PNS) to a black hole is followed using various progenitor models, adopting a hyperonic equation of state (EoS) generated by Shen *et al.* [Shen, Toki, Oyamatsu, and Sumiyoshi, *Astrophys. J., Suppl. Ser.* **197**, 20 (2011)]. The results are compared with those of a nuclear EoS by Shen *et al.* [Shen, Toki, Oyamatsu, and Sumiyoshi, *Nucl. Phys. A* **637**, 435 (1998)] to understand the role of Λ hyperons in the core-collapse supernova. The neutrino signals that may be used as a probe for core collapse is also discussed. Further, an exotic EoS may support a cold neutron star with a maximum mass much lower than that of a PNS. In this regard, the metastability of a PNS in the presence of Λ hyperons is studied in the long-time evolution of the progenitors, relevant to supernova SN1987A.

DOI: [10.1103/PhysRevC.89.035807](https://doi.org/10.1103/PhysRevC.89.035807)

PACS number(s): 26.60.Kp, 26.50.+x, 14.20.Jn

I. INTRODUCTION

The study of hot and dense matter relevant to neutrons stars is an interesting problem. Apart from conventional nuclear matter, the neutron star core might contain exotic matter such as hyperons, quarks, and Bose-Einstein condensates of antikaons at higher densities [1]. It is obvious that the inclusion of strange degrees of freedom softens the equation of state (EoS). A stiffer EoS can result in higher maximum mass neutron stars. A soft EoS, on the other hand, favors lower maximum masses compared to the stars having nucleonic degrees of freedom only. The recent measurement of the Shapiro delay in the radio pulsar PSR J1614–2230 which yielded a mass of $1.97 \pm 0.04 M_{\odot}$ [2] and the mass measurement of PSR J0348+0432 having mass $2.01 \pm 0.04 M_{\odot}$ [3] put an important constraint on the neutron star mass and may rule out most of the soft EoS. However, at present it is not possible to rule out any exotica with this observation because many model calculations including Λ hyperons and/or quark matter could still be compatible with the observations [4–6]. Many of these approaches are parameter dependent; for example, the EoS with Λ hyperons [7] are compatible with the benchmark of $2M_{\odot}$.

EoS provide crucial nuclear physics input to the core-collapse supernova simulations. Generating a finite-temperature EoS table that covers a wide range of density (10^4 – 10^{15} g/cm³), temperature (0–100 MeV), and composition (proton fraction 0–0.6) is indeed a challenging task. Also subsaturation density regions containing nuclei and nonuniform nuclear matter relevant to crust of neutron stars should be carefully matched with the high-density EoS. Mainly two EoS, Lattimer-Swesty (LS) [8] and Shen *et al.* (Shen hereafter) [9], are widely used for supernova simulations. These contain nonstrange particles like neutrons, protons, α particles, and nuclei. The LS EoS is based on the nonrelativistic liquid-drop model while the Shen EoS is computed in the framework of the relativistic mean field (RMF) with the TM1 parameter set [10] taking into consideration the Thomas-Fermi approximation.

Both the models are worked out in a single representative nucleus and in α particles of light clusters; no shell effect is considered. Other notable nucleonic EoS are based on thermodynamically consistent nuclear statistical equilibrium and RMF models [11,12] and virial expansion methods [13]. The first EoS with non-nucleonic degrees of freedom was presented by Ishizuka *et al.* [14]. They studied the emergence of the full baryon octet in the dynamical collapse of a massive static star to a black hole (BH) [15]. This EoS was utilized to study the behavior of black hole formation and neutrino emission with hyperons and/or pions in Ref. [16]. Recently stellar core collapse simulations were reported with additional pions and Λ particles in LS EoS [7]. Shen *et al.* extended their nuclear EoS [9] to include hyperon degrees of freedom in the RMF framework [4], which is eventually used for the supernova simulations and labeled as $np\Lambda$ EoS in this paper.

Neutrinos are very important observables for the core-collapse supernova explosions. The massive stars at their final journey implode so quickly that the inner core rebounds; a shock wave is said to form [17]. After the core bounce, trapped neutrinos diffuse out of the core and escape the surface of the star, which can be recorded by the detectors on earth. The neutrinos carry off most of the energy; the shock soon loses its power and stalls after traversing a few hundred kilometers [17]. The neutrino signals cease. There are different ideas to revive the shock, which could trigger a delayed supernova explosion. One such idea is a quark-hadron phase transition in the high-density core of the compact star [18]. This would be manifested by a subsequent set of neutrino bursts.

SN1987A, since its discovery, has become the most studied star remnant in history and has provided great insights into supernovae and their remnants. The observation of a burst of neutrino signal for at least 12 s after the explosion strongly supports the scenario that a protoneutron star (PNS) was initially present in the core that then cooled via neutrino emission and collapsed later. The fading light curve also lends support to this picture. During deleptonization, the hot and neutrino-trapped PNS may end up forming either a cold neutron star (CNS) or a BH. To date astronomers have not been able to find a neutron star in the remnant of this type

*sarmistha.banik@hyderabad.bits-pilani.ac.in

II supernova. However, the existence of a metastable PNS at least 12 s after the explosion indicates some deep physical implications [19,20].

It is believed that the fate of the compact object depends on the EoS and the amount of infalling material. The general-relativistic calculations limit a maximum mass that can be sustained by an EoS [21]. There are two possible scenarios of formation of BHs after the supernova explosion. If the BH formation time is comparable to the accretion time, the PNS must have accreted sufficient mass on that time scale to overshoot the maximum limit set by the EoS [22]. However, a delayed BH formation indicates the metastability in neutron stars on the deleptonization time scale, which is consistent with the observation of SN1987A. Strangeness could be the reason for such a delay in BH formation [23–25]. Strange matter, which is believed to exist in the high-density core of neutron stars [1], might already exist in the early postbounce phase of a core-collapse supernova. It is explored if strange Λ hyperons can drive the BH formation in the long-time evolution of the PNS, e.g., 12 s as in SN1987A.

It has been reported by several authors that PNSs made up of nucleons have a maximum mass slightly smaller than that of the neutrons stars [19,25,26]. Bethe and Brown calculated the maximum mass of a CNS, which is known as the Bethe-Brown limit ($1.56M_{\odot}$) [20]. A PNS with exotic matter may have a maximum mass larger than that of a CNS and the Bethe-Brown limit, a reversal of the conventional nuclear matter scenario [19,20]. Because baryonic mass is conserved, once sufficient thermal support is lost with cooling, the PNS becomes metastable and it collapses to a low-mass BH. The delayed collapse to a BH has been studied using a hyperon EoS [27,28]. However, the hyperon EoS used in these cases was not a state-of-the-art EoS like Shen hyperon EoS [4].

In this paper, the influence of Λ hyperons on the BH formation is reported using the spherically symmetric general-relativistic hydrodynamic code GRID [29]. The code is designed to follow the evolution of stars beginning from the onset of core collapse. Two Shen EoS, one for nucleon (np) [9] and one for Λ hyperon ($np\Lambda$) degrees of freedom [4], have been used. The neutrino signal that might be observed as a result of phase transition from nucleonic to hyperonic matter is discussed. Finally, the problem of metastability of the PNS in SN1987A is addressed and whether Λ hyperons can delay the BH formation for a while (~ 12 s) is investigated. The paper is arranged as follows. In Sec. II, the EoS and GRID code are briefly described. Section III is devoted to results and discussion. Finally in Sec. IV the paper is summarized.

II. THE EOS AND THE NUMERICAL SIMULATION

Here the nuclear and hyperon EoS by Shen *et al.* [4,9] are used for simulations. The Shen nuclear EoS is based on a RMF model at intermediate and high densities ($\rho > 10^{14.2}$ g/cm³). At low temperature ($T \leq 14$ MeV) and $\rho < 10^{14.2}$ g/cm³, the Thomas-Fermi approximation is used. The nonuniform matter at low temperature and density is modeled to consist of free nucleons, α particles, and heavy nuclei, whereas at extremely low density ($\rho < 10^{10}$ g/cm³) and finite temperature a uniform nucleon gas of n , p , and α particles is considered. Leptons

are treated as uniform noninteracting relativistic particles and their contributions are added separately. Minimization of free energy is done both for nonuniform matter and uniform nucleon gas at low density. For $\rho > 10^{14.2}$ g/cm³, the calculation has been done using a finite temperature, field-theoretical RMF model in which the interactions among baryons are mediated by the exchange of σ , ω , and ρ mesons. The model Lagrangian is of the following form:

$$\begin{aligned} \mathcal{L} = & \sum_{B=N,\Lambda} \bar{\psi}_B (i\gamma_{\mu} \partial^{\mu} - m_B + g_{\sigma B} \sigma - g_{\omega B} \gamma_{\mu} \omega^{\mu} \\ & - g_{\rho B} \gamma_{\mu} \vec{\tau}_B \cdot \vec{\rho}^{\mu}) \psi_B + \frac{1}{2} \partial_{\mu} \sigma \partial^{\mu} \sigma - \frac{1}{2} m_{\sigma}^2 \sigma^2 \\ & - \frac{1}{3} g_2 (\sigma)^3 - \frac{1}{4} g_3 (\sigma)^4 - \frac{1}{4} \omega_{\mu\nu} \omega^{\mu\nu} + \frac{1}{2} m_{\omega}^2 \omega_{\mu} \omega^{\mu} \\ & + \frac{1}{4} c_3 (\omega_{\mu} \omega^{\mu})^2 - \frac{1}{4} \rho_{\mu\nu} \cdot \rho^{\mu\nu} + \frac{1}{2} m_{\rho}^2 \rho_{\mu} \cdot \rho^{\mu}, \quad (1) \end{aligned}$$

where ψ_B denotes the baryon field B , and σ , ω_{μ} , and $\rho_{\mu\nu}$ are the fields of σ , ω , and ρ mesons with masses m_{σ} , m_{ω} , and m_{ρ} , respectively. The field strength tensors for the vector mesons are given by $\omega^{\mu\nu} = \partial^{\mu} \omega^{\nu} - \partial^{\nu} \omega^{\mu}$ and $\rho^{\mu\nu} = \partial^{\mu} \rho^{\nu} - \partial^{\nu} \rho^{\mu}$. In this case, the calculations are done with the TM1 parameter set [10]. The nucleon-meson coupling constants $g_{\sigma B}$, $g_{\omega B}$, and $g_{\rho B}$ are obtained by fitting the experimental data for binding energies and charge radii of heavy nuclei. With the TM1 parameter set, the nuclear matter saturation density is 0.145 fm⁻³, the binding energy per nucleon is 16.3 MeV, the symmetry energy is 36.9 MeV, and the compressibility is 281 MeV [10]. The meson-nucleon parameters for the TM1 model are given in Table I.

One advantage of the RMF model is that it can include hyperons systematically. For their EoS including hyperons, Shen *et al.* use the experimental mass $M_{\Lambda} = 1115.7$ MeV [4]. The coupling constant for Λ hyperon-vector meson interactions is taken based on the naive quark model, whereas the coupling constant for hyperon-scalar meson interactions is determined by fitting experimental binding-energy data for single- Λ hypernuclei [30]. Λ hyperons appear when the threshold condition $\mu_n = \mu_{\Lambda}$ is satisfied at higher density, where μ_n and μ_{Λ} are the chemical potentials of neutrons and Λ hyperons, respectively. Other hyperons, Ξ and Σ , are excluded due to their relatively higher threshold and lack of experimental data [4].

I use the open source code GRID [29] for the supernova simulations. GRID is a spherically symmetric, general-relativistic Eulerian hydrodynamics code for low- and intermediate-mass progenitors. It is designed to follow the evolution of stars beginning from the onset of core collapse to BH formation and makes use of several microphysical EoS. Neutrino effects are crucial in stellar collapse; they are the source of both cooling and heating [29]. Here neutrinos other than the electron type (ν_e) and antielectron type ($\bar{\nu}_e$) are grouped as ν_x . So, three sets of neutrino species, ν_e , $\bar{\nu}_e$, and $\nu_x = (\nu_{\mu}, \bar{\nu}_{\mu}, \nu_{\tau}, \bar{\nu}_{\tau})$, are considered. Neutrino emission takes place when electrons are captured by free or bound protons leading to a decrease in the lepton number. In this code, the lepton fraction is parametrized as a function of density according

TABLE I. Parameters of the meson-nucleon couplings in the TM1 model [4].

m_B (MeV)	m_σ (MeV)	m_ω (MeV)	m_ρ (MeV)	$g_{\sigma B}$	$g_{\omega B}$	$g_{\rho B}$	g_2 (fm ⁻¹)	g_3	c_3
938.0	511.197 77	783.0	770.0	10.028 92	12.613 94	4.632 19	-7.232 47	0.618 33	71.307 47

to Liebendörfer's prescription [31]. However, postbounce, it cannot capture the effect of neutrino cooling, deleptonization, or neutrino heating. Hence a three-flavor, energy-averaged neutrino leakage scheme is adopted [29]. This captures the effects of cooling. The leakage scheme provides the approximate energy and the emission rates. Neutrino heating is included via a parametrized charged-current heating scheme based on Ref. [32]. The heating rate at radius r is given by

$$Q_{\nu_i}^{\text{heat}}(r) = f_{\text{heat}} \frac{L_{\nu_i}(r)}{4\pi r^2} \sigma_{\text{heat}, \nu_i} \frac{\rho}{m_u} X_i \left\langle \frac{1}{F_{\nu_i}} \right\rangle e^{-2\tau_{\nu_i}}, \quad (2)$$

where $L_{\nu_i}(r)$ is the neutrino luminosity inside radius r , τ_{ν_i} is the optical depth, determined through the leakage scheme, $\sigma_{\text{heat}, \nu_i}$ is the energy-averaged absorption cross section, $X_i (i = p, n)$ is the mass fraction of the protons and neutrons in the neutrino capture reaction, and $\langle 1/F_{\nu_i} \rangle$ is the mean inverse flux factor. One can adjust the neutrino heating in the simulation through the scale factor f_{heat} . See Ref. [29] for a detailed discussion. $f_{\text{heat}} = 1$ is taken, if not mentioned otherwise.

III. RESULTS AND DISCUSSION

The Tolman-Oppenheimer-Volkov equations for the zero temperature ($T = 0$) EoS of neutron stars are solved assuming neutrinoless β equilibrium. The maximum mass of the neutron star for the np EoS is $2.18M_\odot$, whereas for the $np\Lambda$ EoS, the

TABLE II. BH formation time and maximum mass of PNS (both baryonic and gravitational) for $f_{\text{heat}} = 1$ for the np and $np\Lambda$ EoS of Shen *et al.* [4,9] and for different progenitor models of Woosley and Heger [33].

Model	t_{bounce} (s)	np			$np\Lambda$		
		t_{BH} (s)	$M_{b,\text{max}}$ (M_\odot)	$M_{g,\text{max}}$ (M_\odot)	t_{BH} (s)	$M_{b,\text{max}}$ (M_\odot)	$M_{g,\text{max}}$ (M_\odot)
S15WH07	0.174	2.810	2.192	2.039	2.814	2.183	2.031
S20WH07	0.232	2.360	2.420	2.243	1.612	2.212	2.083
S23WH07	0.266	1.623	2.594	2.461	0.847	2.304	2.19
S25WH07	0.235	2.060	2.481	2.299	1.377	2.225	2.104
S30WH07	0.203	2.809	2.306	2.142	2.260	2.20	2.06
S35WH07	0.241	2.121	2.620	2.420	2.125	2.591	2.40
S40WH07	0.273	1.085	2.706	2.554	0.565	2.384	2.336
S45WH07	0.262	2.104	2.612	2.448	1.171	2.661	2.483
S50WH07	0.190	2.510	2.285	2.129	2.114	2.19	2.057
S55WH07	0.172	2.460	2.279	2.120	2.260	2.162	2.030
S60WH07	0.188	3.060	2.158	2.011	3.212	2.142	1.999
S70WH07	0.221	2.860	2.339	2.167	2.197	2.162	2.030
S80WH07	0.210	3.060	2.556	2.094	2.113	2.134	2.001

maximum mass reduces to $1.82M_\odot$. The corresponding radii are 12 and 12.5 km, respectively.

The core-collapse supernova simulation starts with the gravitational collapse of the iron core of a progenitor model adopted as an initial model and EoS enter as inputs into general-relativistic hydrodynamics. The simulations are performed with $f_{\text{heat}} = 1$ for several progenitor models of Woosley and Heger [33] using GRID [29] and for the Shen EoS— np and $np\Lambda$ EoS [4,9]; the bounce time, BH formation time, and maximum baryonic and gravitational mass of PNS are tabulated in Table II. The BH formation time is quoted postbounce, not in real time, unless mentioned otherwise. It is observed that the maximum mass is higher than that of neutron stars. The simulations are run until postbounce 3.5 s assuming they might have exploded in nature by this time [29]. When accretion pushes a PNS over its maximum mass, a BH is formed. In Fig. 1, the temporal evolution of the baryonic and gravitational mass of PNSs are plotted for progenitor models, $40M_\odot$ and $23M_\odot$. The bounce corresponds to the spikes in the gravitational mass, and maximum baryonic and gravitational mass of PNS are tabulated in Table II. The BH formation time is quoted postbounce, not in real time, unless mentioned otherwise. It is observed that the maximum mass is higher than that of neutron stars. The simulations are run until postbounce 3.5 s assuming they might have exploded in nature by this time [29]. When accretion pushes a PNS over its maximum mass, a BH is formed. In Fig. 1, the temporal evolution of the baryonic and gravitational mass of PNSs are plotted for progenitor models, $40M_\odot$ and $23M_\odot$. The bounce corresponds to the spikes in the gravitational mass, and maximum baryonic and gravitational mass of PNS are tabulated in Table II.

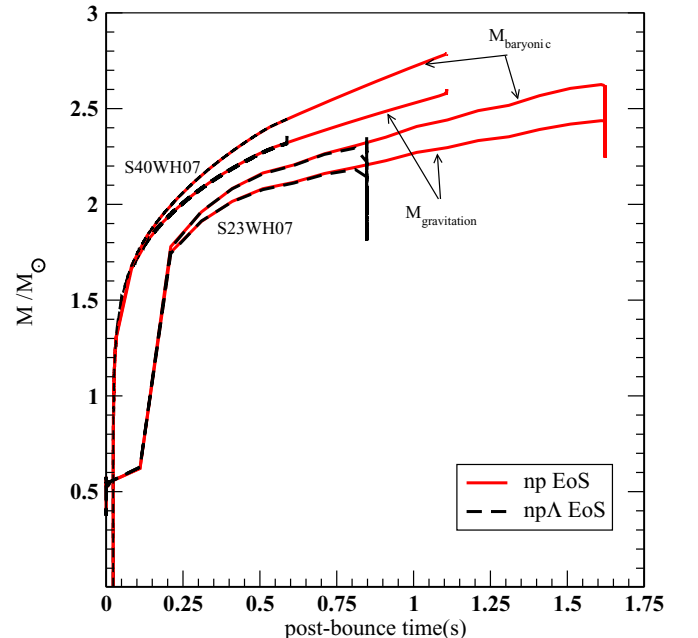


FIG. 1. (Color online) Temporal evolution of baryonic and gravitational mass for the Shen np and $np\Lambda$ EoS.

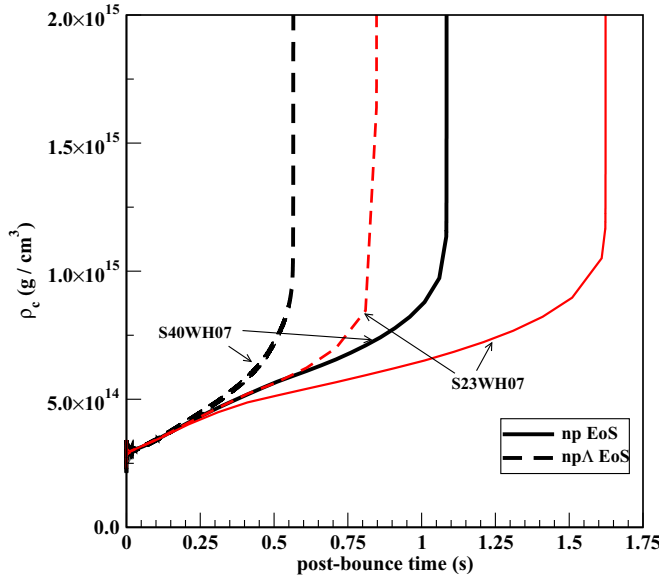


FIG. 2. (Color online) Temporal evolution of central density for the Shen np and $np\Lambda$ EoS.

accounts for the lower gravitational mass compared to the total mass of all its constituents, i.e., baryonic mass. Dashed dark lines (solid, color online) are used for the $np\Lambda$ (np) EoS. For the np EoS, the BH is formed with a baryonic mass of $2.706M_{\odot}$ at 1.085 s postbounce, whereas for the $np\Lambda$ EoS (the dashed lines) this happens much earlier at 0.565 s postbounce for a baryonic mass of $2.384M_{\odot}$. Strangeness degrees of freedom soften the EoS and in the process can support less mass against gravity compared to nonstrange stars. Continued accretion thus overshoots the maximum mass early. In other words, the stiffer EoS leads to a longer postbounce time to BH formation. This is compared with the results of a $23M_{\odot}$ progenitor (the lower set of lines in Fig. 1). The PNS mass is much less than that of the $40M_{\odot}$ progenitor. Also, in this case the PNS accretes matter for a longer time until it blows as a BH at 1.623(0.847) s postbounce for the np ($np\Lambda$) EoS, the maximum baryonic mass being 2.594(2.304) M_{\odot} . Here also Λ hyperons are shown to hasten the BH formation.

Figures 2 and 3 show the time evolution of the central density (ρ_c) and the temperature (T), respectively, for the np and $np\Lambda$ EoS in the two panels. Here dark lines (color online) are used to distinguish $40M_{\odot}$ and $23M_{\odot}$ progenitors. The onset of BH formation is marked by a sharp rise in the value of ρ_c and T . The central density just before BH formation reaches about 10^{15} g/cm³ and the temperature varies from 22 to 32 MeV for the np and $np\Lambda$ EoS for both the progenitors. Owing to the hyperon emergence, the contraction of the PNS is accelerated, which leads to a quicker rise in the temperature and the central density.

In Fig. 4, the density profiles of the PNS are compared for the np and $np\Lambda$ cases in the two panels. Colored lines (online) are used for the $23M_{\odot}$ progenitor. For the $40M_{\odot}$ progenitor, it is noted that the density rises from less than normal nuclear matter density ($\rho_0 \simeq 2.4 \times 10^{14}$ g/cm³) at the surface to a few times ρ_0 at the core. The plateau in the midradius region

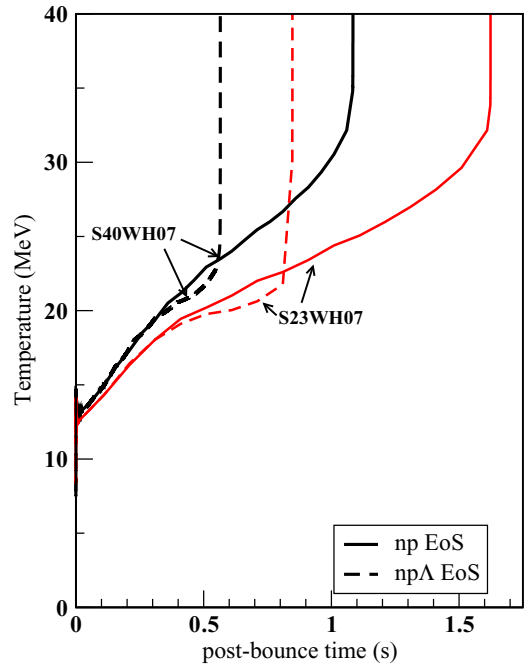


FIG. 3. (Color online) Temporal evolution of temperature for the Shen np and $np\Lambda$ EoS.

could be attributed to strong thermal pressure as is evident in Fig. 5. At core bounce, the central density is $1.4\rho_0$. With intense accretion, the central density shoots to $\sim 2\rho_0$ at 0.363 s and to $2.5\rho_0$ at 0.563 s for the $40M_{\odot}$ progenitor with the np EoS [Fig. 5(a)]. The trend in the density profile remains similar for the np and $np\Lambda$ cases. The central density is slightly above that of the np case at $t = 0.363$ s in the presence of Λ s, which just start appearing in the system. However, at $t = 0.563$ s, owing to a substantial amount of Λ , the central density rises to almost $3.9\rho_0$, which is ~ 2.8 times its value at core bounce [Fig. 5(b)]. Next the density profile is discussed for the $23M_{\odot}$ progenitor, which looks similar to that of the $40M_{\odot}$ progenitor just after the bounce. However differences creep up with time and become much more pronounced in the presence of Λ hyperons. For the np ($np\Lambda$) EoS, at 0.563 s the central density rises to 2.2 (2.5) ρ_0 compared to 2.5 (3.9) ρ_0 for the $40M_{\odot}$ case. Just before BH formation (at ~ 0.847 s) the central density reaches $3.9\rho_0$ for the $np\Lambda$ system. The central density remains at $2.6\rho_0$ for the np system at this instant until it reaches $17\rho_0$ when the BH is formed at 1.623 s (not shown in the figure).

The evolutions of the temperature profiles are compared in the absence and presence of Λ s in Fig. 5. In both cases, the temperature attains a peak at the midradius region. For the $40M_{\odot}$ progenitor the peak rises from 66.8 MeV at 0.363 s to 79.4 MeV at 0.563 s in the np case [Fig. 5(a)]. This is due to the accretion and compression of shock-heated material onto the PNS surface. In this region, the thermal pressure support is enough to flatten the density profile. In the inner core (~ 6 km) the material is not shock heated; rather it is heated by adiabatic compression. The temperature peak is further raised to 91.7 MeV at 0.563 s in the presence of Λ hyperons [Fig. 5(b)]. When compared with a $23M_{\odot}$ progenitor, the rise in temperature

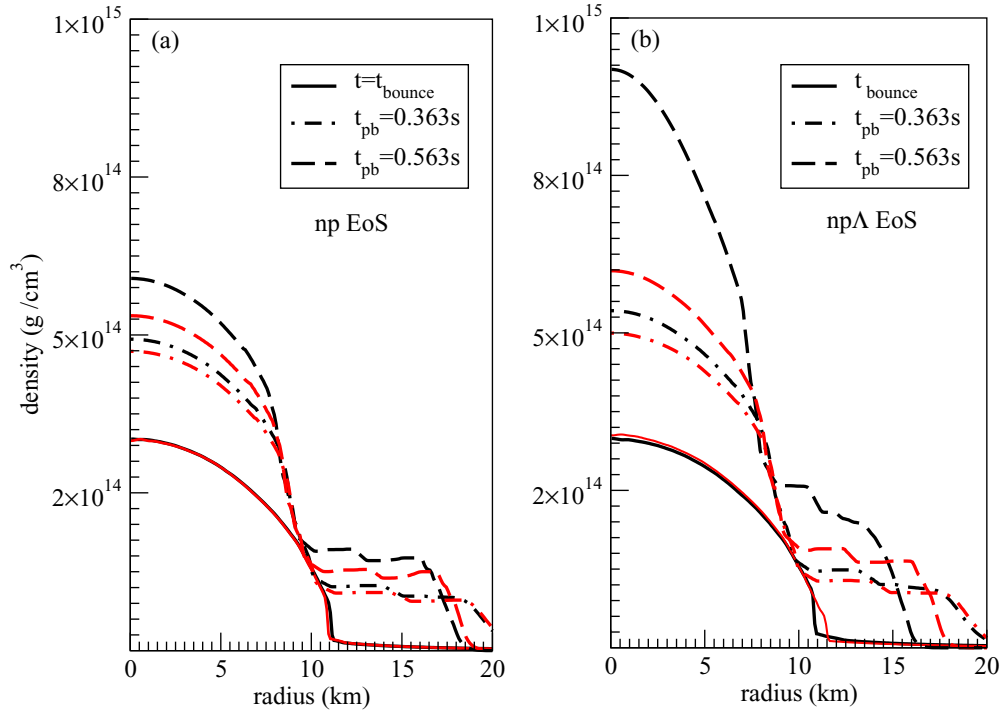


FIG. 4. (Color online) Density profile of the $40M_{\odot}$ (black lines) and $23M_{\odot}$ (red/gray lines) progenitors with np [panel (a)] and $np\Lambda$ [panel (b)] EoS at $t = t_{\text{bounce}}$ and at postbounce times of 0.363 and 0.563 s.

is not so quick. It increases up to 71.5 (74.4) MeV at 0.563 s for np ($np\Lambda$), which accounts for the corresponding lower central density of Fig. 4. But the temperature eventually reaches 80 (169) MeV just before 0.847 s, when the BH is formed for the

$np\Lambda$ system. The temperature peaks at 167 MeV before BH formation for the np system at 1.623 s (not shown in the figure).

Next the compositions of PNS are compared in Figs. 6 and 7. From Fig. 6 it is evident that initially at core bounce

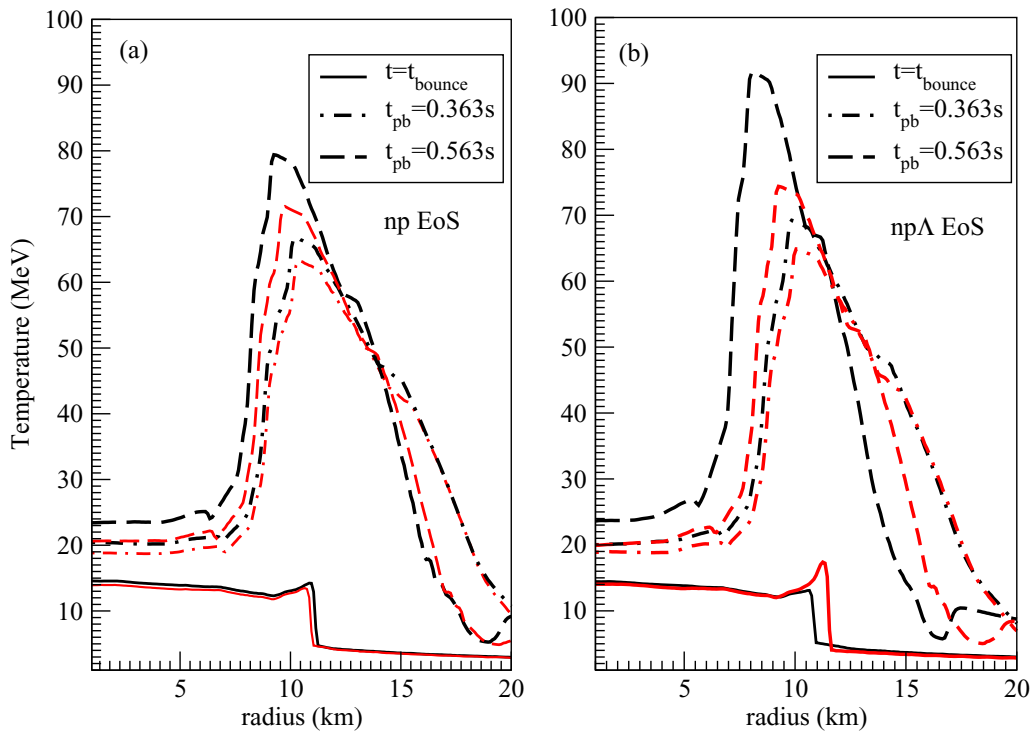


FIG. 5. (Color online) Temperature profile of the $40M_{\odot}$ (black lines) and $23M_{\odot}$ (red/gray lines) progenitors with np [panel (a)] and $np\Lambda$ [panel (b)] EoS at $t = t_{\text{bounce}}$ and at postbounce times of 0.363 and 0.563 s.

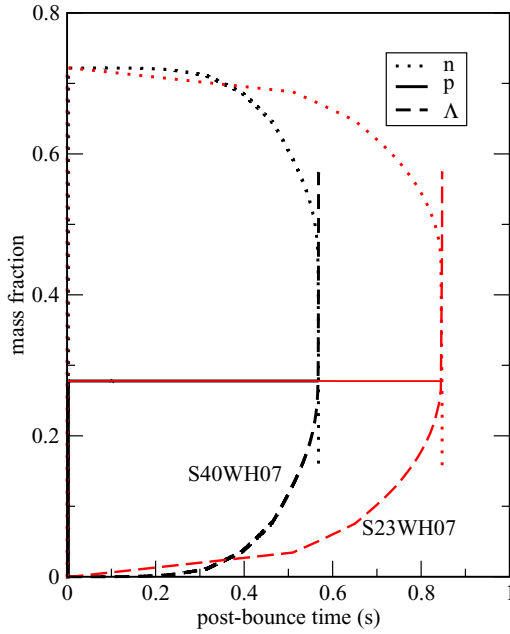


FIG. 6. (Color online) Mass fractions of the constituents for the $40M_{\odot}$ (black lines) and $23M_{\odot}$ (red/gray lines) progenitors with the Shen $np\Lambda$ EoS.

the system consists of neutrons and protons only; Λ hyperons appear first in the collapse at 0.16 s after core bounce (assuming 10^{-3} considerable amount of fraction). The central density that was just above the normal nuclear matter density (see Fig. 2) at bounce rises to $3.79 \times 10^{14} \text{ g/cm}^3 \simeq 1.6\rho_0$ at 0.16 s

after bounce. The temperature also increases to 16.26 MeV. This is on par with our earlier findings that the appearance of Λ hyperons is delayed until the matter density reaches at least $2\rho_0$ at $T = 0$ [26,34] and the threshold density shifts to lower density with increasing temperature [4]. A snapshot of the mass fraction for the $40M_{\odot}$ progenitor at 0.363 and 0.563 s is displayed in Fig. 7(a). It is interesting to note that the Λ hyperons appear off-center owing to high temperature, although the density is still on the plateau. At 0.363 s after core bounce, the abundance of Λ becomes significant at $R \simeq 10$ km, because the temperature is maximum there (Fig. 5). It even falls sharply after reaching the peak due to a fall in temperature, only to rise at the core again owing to the high density there. At a later time, the high central density forbids it from dropping too low, once it reaches the peak at midradius region. Thus, Λ becomes one of the major components in the core. Similar snapshots are drawn for the $23M_{\odot}$ progenitor in the Fig. 7(b) at 0.363 and 0.840 s.

I study the evolution of total neutrino luminosity, which includes contributions from ν_e , $\bar{\nu}_e$, and rest ν_x [35] and find a short neutrino burst (~ 1 s) before the PNS, born temporarily in a failed supernova, terminates in a BH. The resulting neutrino bursts in the np and $np\Lambda$ cases are quite similar, differing only in earlier termination of the burst in the latter. The neutrino burst ceases at 1.085 and 1.623 s postbounce in the np case for the 40 and $23M_{\odot}$ progenitors, respectively. The soft $np\Lambda$ EoS lowers the critical mass of the PNS and thus accelerates the mass accretion onto it and triggers the gravitational instability at 0.565 and 0.847 s postbounce for the 40 and $23M_{\odot}$ progenitors, respectively. However, no second neutrino burst is observed as in the quark-hadron phase transition [18]. It may be

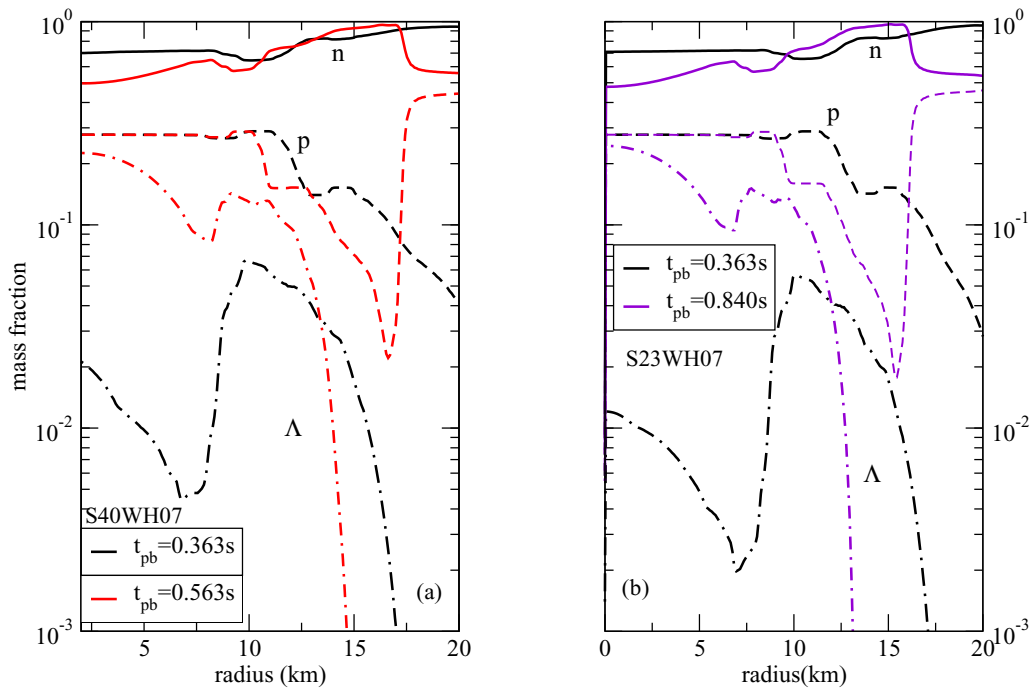


FIG. 7. (Color online) Snapshots of mass fractions of the constituents vs radius at $t = 0.363$ s (black lines) and 0.563 s (red/gray lines) postbounce for the $40M_{\odot}$ progenitors (a) and $t = 0.363$ s (black lines) and 0.84 s (purple/gray lines) postbounce for the $23M_{\odot}$ progenitors (b) with the Shen $np\Lambda$ EoS.

noted that the quark-hadron phase transition was a first-order phase transition [18] whereas the phase transition from nuclear to hyperon matter was a second-order phase transition in the Shen hyperon EoS. The second neutrino burst might be the result of a first-order quark-hadron phase transition.

At this point we recall the observation of burst of 11 and 8 antineutrinos from SN1987A over the time period of ~ 12 s in the underground detectors of Kamiokande II in Japan and IMB in Ohio, respectively. All the evidence reveals that the supernova SN1987A lies at the position of a former, blue supergiant star, Sanduleak-69202 of mass around $20M_{\odot}$. So, did SN1987A create a BH at the end of 11 s when the neutrino signals ceased or did it end up as a neutron star? To explain these observations, the evolution of the progenitors of mass of $\sim 20M_{\odot}$ is followed for 11 s. Because one-dimensional supernova models cannot produce an explosion, the energy deposition is increased by artificially raising the neutrino heating (f_{heat}). The scaling factor f_{heat} of Eq. (2) appears in the parametrized neutrino heating [29,32]. Until now, a standard setting of $f_{\text{heat}} = 1$ was used in the calculations. In this case, once sufficient matter is accreted onto the PNS, it might overshoot the maximum mass that can be supported by the EoS and eventually can collapse into a BH. The motivation here is to study whether the shock can be revived through neutrino heating and whether metastability is a plausible mechanism with Λ hyperons to collapse the PNS into a BH. Ott *et al.* found BH formation for some extreme models within 1 s of the cooling phase for higher values of f_{heat} [36]. In Fig. 8, the shock radii for the $23M_{\odot}$ progenitors are plotted with different values of f_{heat} . For $f_{\text{heat}} > 1$, the shock radii increase with time. It is found that $f_{\text{heat}} = 1.27$ corresponds to the critical value required to cause a successful explosion. The PNS never ceases to accrete mass for values of $f_{\text{heat}} < 1.27$. The density

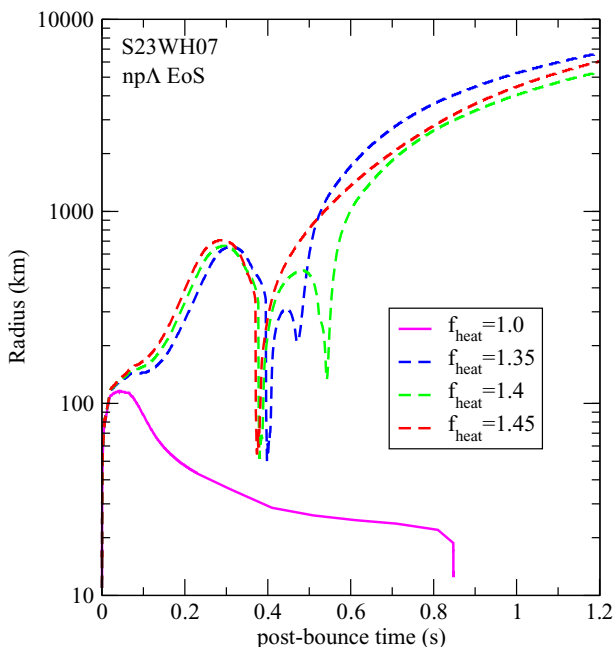


FIG. 8. (Color online) Evolution of shock radii for the $23M_{\odot}$ progenitor models.

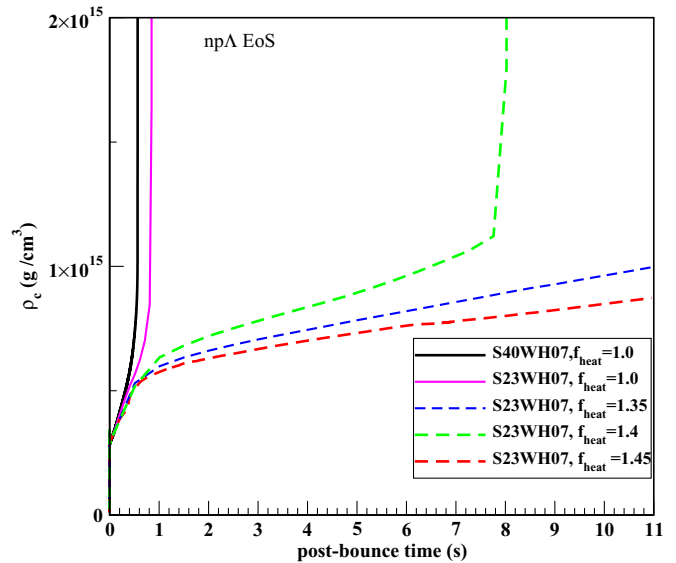


FIG. 9. (Color online) Long-time evolution of central density for the $23M_{\odot}$ progenitor model with the $np\Lambda$ EoS.

and temperature profiles with $f_{\text{heat}} > 1$ are compared to the previous simulations (Figs. 9 and 10). For $f_{\text{heat}} = 1.4$, jumps in the central density and the temperature and delayed BH formation are found at ~ 8 s. In other cases, even after 11 s the PNS remains stable. A similar situation was reported in Ref. [27]. The same feature is evident in the gravitational mass evolution (Fig. 11) also. The solid lines are for the $40M_{\odot}$ and $23M_{\odot}$ progenitors with $f_{\text{heat}} = 1$. The other lines are for $f_{\text{heat}} > 1$ and the $23M_{\odot}$ progenitor. Please note that the metastability of PNS due to hyperons was also explored earlier and the time of instability to BH formation was estimated in Ref. [25].

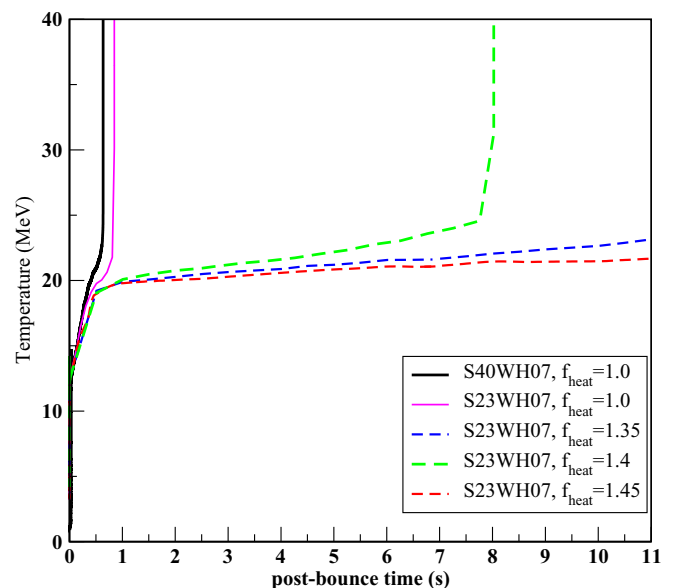


FIG. 10. (Color online) Long-time evolution of temperature for the $23M_{\odot}$ progenitor model with the $np\Lambda$ EoS.

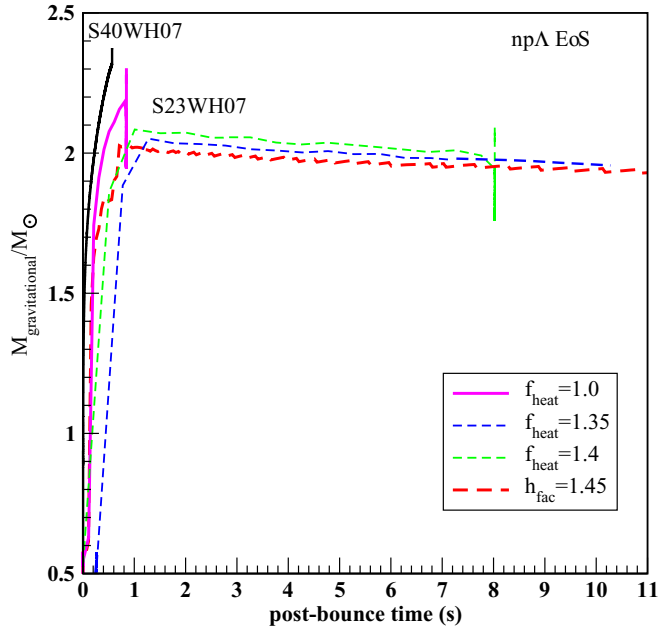


FIG. 11. (Color online) Long-time evolution of gravitational mass for the $23M_{\odot}$ progenitor model with the $np\Lambda$ EoS. The dark solid line is with $f_{\text{heat}} = 1$ for the $40M_{\odot}$ progenitor, and the rest of the lines are for the $23M_{\odot}$ progenitor.

IV. SUMMARY

The effect of the hadron-hyperon phase transition in core-collapse supernovae has been studied here using the general-relativistic hydrodynamic simulation code GRID [29]. Following the dynamical collapse of a newborn PNS from the gravitational collapse of several progenitor stars with the Shen hyperonic EoS table [4], Λ hyperons are observed to appear just after the bounce. They appear off-center at first due to high temperature and prevail at the center of the PNS just before the BH formation, when the density becomes quite high. The $40M_{\odot}$ progenitor models of Woosley and Weaver [37] and Woosley and Heger [33] have been used in core-collapse supernova simulations by several other authors [7, 15, 29, 38, 39] due to their relatively large iron core. Our results for the $40M_{\odot}$ progenitor are compared with those of Sumiyoshi *et al.* [15], who found $t_{\text{BH}} = 0.682$ s with their EoS containing Λ , Σ , and Ξ hyperons. Peres *et al.* [7], however, found $t_{\text{BH}} = 0.2745$ s for LS220 + Λ EoS. For the Shen $np\Lambda$ EoS, BH formation is observed at 0.565 s.

Λ hyperons trigger the BH formation, but fail to generate the second shock because the EoS is softened too much with their appearance. The emergence of Λ hyperons in the collapse produces an intense but short neutrino burst, which terminates

at the BH formation. However, no second neutrino burst is observed as in the quark-hadron phase transition [18]. The fact that the quark-hadron phase transition is of first order and the nucleon-hyperon phase transition in the Shen $np\Lambda$ EoS is of second order might be a possible reason for the no show of a second neutrino burst in the latter case. Also, accurate determination of neutrino fluxes and energy demands the use of better transport calculations than the schemes adopted in GRID.

I report the long-time evolution of the $23M_{\odot}$ progenitor to explain the observations following the advent of supernova SN1987A. With the Shen hyperonic EoS, the maximum gravitational mass of the PNS exceeds that of the neutron star. The PNS cools via neutrinos and, once sufficient thermal support is lost, no stable configuration exists and the PNS might collapse into a BH. Because one-dimensional supernova simulations are unlikely to produce a successful explosion, the amount of neutrino heating has been artificially adjusted via the scale factor f_{heat} to achieve explosions. The delayed collapse of the PNS into a BH has been observed for $f_{\text{heat}} = 1.4$. A more accurate neutrino treatment is needed to investigate the long-time evolution of PNS.

Also, the maximum mass in the Shen $np\Lambda$ EoS is not on par with the latest benchmark observations of neutron star masses [2, 3]. More hyperon physics at high densities is required at this point. Still, the existence of high-mass neutron stars with hyperons is possible in the quark-meson coupling model, the SU(3) nonlinear σ model, the extended RMF model, etc. [40–42]. We are working towards an EoS table with hyperons for supernova simulation with density-dependent couplings [34, 43].

There are possibilities for other strange degrees of freedom in the form of kaon condensates to appear in the highly dense matter. We have seen that such a phase transition can support a maximum mass [19], which is well above $2M_{\odot}$ [2, 3]. It would be intriguing to investigate if a hadron-antikaon condensed matter can generate the second shock and lead to supernova explosion. A successful shock revival would have observational consequences in the form of neutrino signatures. Until now, only one supernova, SN1987A, has been detected by its neutrinos. Post SN1987A, more advanced neutrino facilities, such as ice-cube and super-Kamiokande, are expected to detect the neutrino signals more efficiently and frequently.

ACKNOWLEDGMENTS

I thank Dr. Evan O'Connor and Dr. Christian Ott for their immense help with their code, and I also thank Professor Debades Bandyopadhyay for insightful discussions and for his meticulous feedback on the manuscript.

- [1] N. K. Glendenning, *Compact Stars* (Springer, New York, 1997).
- [2] P. B. Demorest, T. Pennucci, S. M. Ransom, M. S. E. Roberts, and J. W. T. Hessels, *Nature (London)* **467**, 1081 (2010).
- [3] J. Antoniadis *et al.*, *Science* **340**, 6131 (2013).

- [4] H. Shen, H. Toki, K. Oyamatsu, and K. Sumiyoshi, *Astrophys. J., Suppl. Ser.* **197**, 20 (2011).
- [5] J. M. Lattimer and M. Prakash, *From Nuclei to Stars, Festschrift in Honor of G. E. Brown* (World Scientific, Singapore, 2011), p. 275.

- [6] E. Massot, J. Margueron, and G. Chanfray, *Europhys. Lett.* **97**, 39002 (2012).
- [7] B. Peres, M. Oertel, and J. Novak, *Phys. Rev. D* **87**, 043006 (2013).
- [8] J. M. Lattimer and F. D. Swesty, *Nucl. Phys. A* **535**, 331 (1991).
- [9] H. Shen, H. Toki, K. Oyamatsu, and K. Sumiyoshi, *Nucl. Phys. A* **637**, 435 (1998).
- [10] Y. Sugahara and H. Toki, *Nucl. Phys. A* **579**, 557 (1994).
- [11] M. Hempel and J. Schaffner-Bielich, *Nucl. Phys. A* **837**, 210 (2010).
- [12] S. Furusawa, S. Yamada, K. Sumiyoshi, and H. Suzuki, *Astrophys. J.* **738**, 178 (2011).
- [13] G. Shen, C. J. Horowitz, and S. Teige, *Phys. Rev. C* **83**, 035802 (2011).
- [14] C. Ishizuka, A. Ohnishi, K. Tsubakihara, K. Sumiyoshi, and S. Yamada, *J. Phys. G* **35**, 085201 (2008).
- [15] K. Sumiyoshi, C. Ishizuka, A. Ohnishi, S. Yamada, and H. Suzuki, *Astrophys. J. Lett.* **690**, L43 (2009).
- [16] K. Nakazato, S. Furusawa, K. Sumiyoshi, A. Ohnishi, S. Yamada, and H. Suzuki, *Astrophys. J.* **745**, 197 (2012).
- [17] H. A. Bethe, *Rev. Mod. Phys.* **62**, 801 (1990).
- [18] T. Fischer, I. Sagert, G. Pagliara, M. Hempel, J. Schaffner-Bielich, T. Rauscher, F. K. Thielemann, R. Kppeli, G. Martnez-Pinedo, and M. Liebendörfer, *Astrophys. J., Suppl. Ser.* **194**, 39 (2011).
- [19] S. Banik and D. Bandyopadhyay, *Phys. Rev. C* **63**, 035802 (2001).
- [20] G. E. Brown and H. A. Bethe, *Astrophys. J.* **423**, 659 (1994).
- [21] C. Rhoades, Jr. and R. Ruffini, *Phys. Rev. Lett.* **32**, 324 (1974).
- [22] G. E. Brown, S. W. Bruenn, and J. C. Wheeler, *Comments Astrophys.* **16**, 153 (1992).
- [23] M. Prakash, J. R. Cooke, and J. M. Lattimer, *Phys. Rev. D* **52**, 661 (1995); D. P. Menezes and C. Providência, *Phys. Rev. C* **69**, 045801 (2004).
- [24] J. A. Pons, A. W. Steiner, M. Prakash, and J. M. Lattimer, *Phys. Rev. Lett.* **86**, 5223 (2001).
- [25] J. A. Pons, S. Reddy, M. Prakash, J. M. Lattimer, and J. A. Miralles, *Astrophys. J.* **513**, 780 (1999); J. A. Miralles, J. A. Pons, and J. M. Ibáñez, *Nucl. Phys. B (Proc. Suppl)* **93**, 54 (2001).
- [26] S. Banik and D. Bandyopadhyay, *Phys. Rev. C* **64**, 055805 (2001).
- [27] W. Keil and H.-Th. Janka, *Astron. Astrophys.* **296**, 145 (1995).
- [28] T. W. Baumgarte, H. T. Janka, W. Keil, S. L. Shapiro, and S. A. Teukolsky, *Astrophys. J.* **468**, 823 (1996).
- [29] E. O'Connor and C. D. Ott, *Astrophys. J.* **730**, 70 (2011).
- [30] H. Shen, F. Yang, and H. Toki, *Prog. Theor. Phys.* **115**, 325 (2006).
- [31] M. Liebendörfer, *Astrophys. J.* **633**, 1042 (2005).
- [32] H. Th. Janka, *Astron. Astrophys.* **368**, 527 (2001).
- [33] S. E. Woosley and A. Heger, *Phys. Rep.* **442**, 269 (2007).
- [34] S. Banik and D. Bandyopadhyay, *Phys. Rev. C* **66**, 065801 (2002).
- [35] S. Banik, *J. Phys: Conf. Ser.* **426**, 12004 (2013).
- [36] E. O'Connor and C. D. Ott, *PoS (NIC XI)*, 154 (2011).
- [37] S. E. Woosley and T. A. Weaver, *Astrophys. J. Suppl. Ser.* **101**, 181 (1995).
- [38] M. Hempel, T. Fischer, J. Schaffner-Bielich, and M. Liebendörfer, *Astrophys. J.* **748**, 70 (2012).
- [39] A. W. Steiner, M. Hempel, and T. Fischer, *Astrophys. J.* **774**, 17 (2013).
- [40] V. Dexheimer and S. Schramm, *Astrophys. J.* **683**, 943 (2008).
- [41] S. Weissenborn, D. Chatterjee, and J. Schaffner-Bielich, *Phys. Rev. C* **85**, 065802 (2012).
- [42] S. Weissenborn, D. Chatterjee, and J. Schaffner-Bielich, *Nucl. Phys. A* **881**, 62 (2012).
- [43] S. Typel, G. Röpke, T. Klähn, D. Blaschke, and H. H. Wolter, *Phys. Rev. C* **81**, 015803 (2010).